Graphene Catalysis Made Easy

Amir Karton, School of Science and Technology, University of New England, Armidale, NSW, Australia

Abstract

Catalysis by pristine 2D materials is an emerging form of eco-friendly, heterogeneous catalysis. We review recent computational studies in the field of pristine-graphene catalysis, in which graphene efficiently catalyzes chemical processes via π-interactions and shape complementarity. These include the (1) bowl-to-bowl inversion of curved aromatic molecules (e.g., corannulene and sumanene), (2) enantiomerizations of biaryl compounds (e.g., biphenyl and binaphthyl derivatives), and (3) skeletal inversions of helicenes and cyclooctatetraene derivatives. A pristine graphene catalyst reduces the reaction barrier heights for these processes by amounts ranging from 10 to 50 kJ mol^{-1}, which correspond to reaction rate enhancements by 2–10 orders of magnitude at room temperature. The graphene-catalyzed enantiomerization of BINOL has been confirmed experimentally through chiral HPLC measurements. We highlight potential applications of pristine-graphene catalysis in (1) the dynamic kinetic resolution of biaryls and (2) the directional self-assembly of bowl-shaped aromatic molecules across the graphene monolayer.

Key Points

- Pristine 2D catalysts are emerging as eco-friendly alternatives to homogeneous metal catalysts
- Pristine 2D catalysts do not require monolayer functionalization
- This chapter reviews recent advances in catalysis by pristine graphene
- Pristine graphene catalyzes chemical reactions via dispersion and electrostatic interactions
- Pristine graphene catalyzes the racemization reactions of synthetic relevance
- Pristine graphene catalyzes bowl-inversions of curved aromatic molecules leading to directional self-assembly across the monolayer

1 Introduction

1.1 Overview of Applications of Graphene in Catalysis

The discoveries of new allotropes of carbon with low dimensionalities over the past three decades – buckminsterfullerene,[1,2] single-walled carbon nanotubes,[3,4] and single-layer graphene[5–8] – have defined the field of nanotechnology. Each of these discoveries has led to the birth of a flourishing subfield in nanotechnology. Indeed, over the past two decades, fullerenes, nanotubes, graphene, and their functionalized derivatives have found numerous applications across many branches of physics, chemistry, biology, engineering, pharmacy, agriculture, and textiles, to name a few.[9–27] This chapter provides an overview of applications of pristine graphene in chemical catalysis.

Graphene is an atom-thick two-dimensional (2D) material composed of sp^2-hybridized carbons. Graphene was discovered at the beginning of this century by Andre Geim and Konstantin Novoselov at the University of Manchester. The 2010 Nobel Prize in Physics recognized this discovery. Remarkably, graphene was discovered while trying to answer a simple question: how thin can graphite be made? For decades, sticky tape has been applied to graphite to clean its surface before microscopy work. However, in a purely curiosity-driven experiment, the sticky tape was placed under the microscope instead of the clean surface of graphite, and a thin graphite film consisting of only several layers of graphene was observed.[5–7] The tape dispenser and the lump of graphite are now

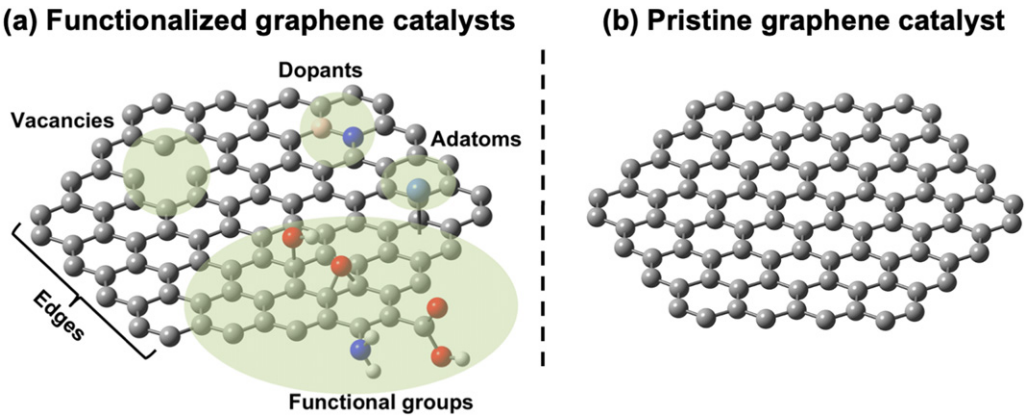

Fig. 1 (a) Functional sites on graphene where catalysis can occur (e.g., defects, dopants, adatoms, and oxidized functional groups). (b) Readily available pristine graphene catalyst.

displayed at the Nobel Museum in Stockholm. Before this discovery, it was believed that a two-dimensional form of carbon could not exist because it would be thermodynamically unstable compared with other forms of carbon, such as graphite, fullerenes, and nanotubes. The discovery of graphene has sparked the imagination of scientists worldwide. Shortly after its discovery, it was realized that graphene bears not only academic significance but also has exceptional physical, optical, thermal, electrical, and chemical properties.[5–9,19,20,22–27] For example, graphene is amongst the thinnest and strongest possible materials, it is both stiffer and thermally more conductive than diamond, has a higher electrical conductivity than copper, and is remarkably flexible. Graphene also has a large surface area (up to $\sim 3000\ m^2\ g^{-1}$), meaning that ~ 10 kg of graphene would cover the entire surface of the moon.

The remarkable physical and chemical properties of graphene, and in particular, its 2D structure, large surface area, and ease of chemical functionalization, make graphene an ideal catalyst support nanomaterial for various chemical processes, ranging from organic synthesis to polymerization reactions.[19,28–37] Graphene-based heterogeneous catalysts provide eco-friendly alternatives for traditional homogeneous catalysts such as metal-based and Brønsted/Lewis acid catalysts. This may have significant industrial implications since heterogeneous catalysts (that is, catalysts that are insoluble in the reaction mixture) are much easier to separate and reuse compared with homogeneous catalysts (that is, catalysts that are soluble in the reaction mixture). Graphene-based materials are also attracting increasing attention due to the ease by which they can interact with polymers, organic dyes, enzymes, and proteins through covalent and noncovalent interactions. New catalytic applications of these materials are continuously being reported in the literature. The present chapter focuses on applications of pristine graphene in catalysis; for in-depth overviews of functionalized graphene-based catalysts, the reader is referred to several excellent reviews published over the past decade.[19,28–37]

Fig. 1 illustrates the various ways in which graphene can be chemically functionalized. In functionalized graphene, catalysis can occur at defect sites (e.g., hole vacancies and edges), heteroatom dopants (e.g., N, B, and P), adatoms adsorbed on graphene (e.g., D- and p-block elements), and functional groups such as those present in graphene oxide (GO) and reduced GO (rGO).[38–40] For example, the functional groups in GO, such as epoxides, hydroxyls, carbonyls, carboxyls, and lactols, can catalyze a range of oxidation reactions, including the selective oxidation of olefins, alcohols, thiols, and sulfides.[30,41–44] GO has also been shown to catalyze Friedel–Crafts reactions, Michael additions, and ring-opening polymerizations.[38,42–44] Another class of highly successful graphene-based catalysts is graphene/transition metal composites.[19,28,29,33,34] For example, the platinum/graphene composite can catalyze methanol oxidation and oxygen reduction reactions in fuel cells. Similarly, it has been found that palladium and gold nanoparticles dispersed on GO can catalyze the Suzuki cross-coupling reaction. This coupling reaction is among the most widely used for the formation of carbon–carbon bonds.[19,44] As a side note, it is worth mentioning that Akira Suzuki received the Nobel Prize in Chemistry in 2010, the same year Andre Geim and Kostya Novoselov received the Nobel Prize in Physics for the discovery of graphene.

It is important to note, however, that in the above functionalized-graphene catalysts, the pristine part of graphene does not play an active role in catalysis but is the catalyst support. Whilst the pristine part of graphene serves as a highly effective catalyst support nanomaterial, the underlying mechanisms for the synthesis of GO and rGO remain elusive, and the structure of functionalized graphene catalysts such as GO is not well understood.[19,28,30,34] A potential limiting factor in the application of such graphene-based catalysts is the lack of a uniform or well-determined structure and the synthetic challenges associated with controlling the distribution of defects, vacancies, dopants, adatoms, and functional groups across the monolayer. As pointed out by De Feyter and coworkers,[45] the non-quantification and variability of the functionals groups incorporated in GO and rGO may lead to low reproducibility of the catalytic effects, and the difficulty in identifying the exact source of the catalytic effect hinders the rational design of new catalysts. Pristine graphene (or other pristine 2D materials), on the other hand, does not suffer from such limitations since it has a well-defined structure and may serve as a readily available catalyst (Fig. 1(b)). Over the past decade, catalysis by pristine graphene (or other 2D materials) has emerged as an exciting form of catalysis with several applications.[45,46]

1.2 Role of van der Waals interactions in Catalysis

Van der Waals (vdW) interactions play a prominent role in supramolecular chemistry and nanomaterials,[19,28,33,47–58] as well as in organic, organometallic, and supramolecular catalysis.[51–58] Of particular relevance to the present review is catalysis or increased selectivity in the presence of graphite.[45,59–61] Since vdW interactions accumulate, they are expected to play an increasingly important role with larger molecular substrates. This is illustrated for π-π interactions by examining the binding energies between increasingly larger aromatic dimers. For example, the binding energies for a series of aromatic parallel displaced (PD) dimers amount to 10.7 (benzene PD dimer),[62] 24.9 (naphthalene PD dimer),[63] and 83.6 (coronene PD dimer) kJ mol^{-1}. [64] These binding energies are calculated using high-level coupled cluster methods (e.g., at the CCSD(T) or CCSDT(Q) levels) and are expected to have chemical accuracy, defined as errors below $\sim$0.4 kJ mol^{-1} for weak interactions.[65] It should be noted that the binding energy between graphene and each of the above molecules (benzene, naphthalene, and coronene) is expected to be significantly higher than the above binding energies in the dimers. For example, a recent density functional theory (DFT) study found that the binding energy between graphene and benzene is approximately 4–5 times larger than the binding energy of the benzene dimer.[66] The binding energy for the circumcoronene dimer cannot be obtained using high-level coupled cluster methods of theory; nevertheless, it is expected to exceed 200 kJ mol^{-1}.[67] Overall, the above results demonstrate that π-π interactions between graphene and polycyclic aromatic systems can exceed the energies required for bond rotation and breaking in organic systems.

1.3 Role of Shape Complementarity in Catalysis

Shape complementarity between the catalyst and transition structure is one of the cornerstones of chemical catalysis.[46,68–79] This concept was initially proposed by Pauling in 1948 in the context of enzymatic catalysis,[68] and was soon after adopted for explaining rate accelerations of a wide range of enzymatic reactions.[69,73] In an elegant application of this concept,[70] Houk, Hilvert, and co-workers rationalized the catalytic mechanism of the highly efficient antibody catalyst for a Diels–Alder reaction (Antibody 1E9).[80] Based on X-ray structure analysis and extensive DFT and docking calculations, Houk, Hilvert, and co-workers were able to show that the close shape complementarity between the transition structure and binding pocket underlines the catalytic function and selectivity of the Diels-Alderase antibody.[70,71] Importantly, this work illustrates that shape complementarity plays a critical role in catalytic processes involving a transition structure with little charge separation or directional interactions (e.g., hydrogen bonds). The next section focuses on how chemical processes that involve transition structures with little or no charge separation can be catalyzed by pristine 2D graphene via shape complementarity and π-π interactions.

Induced-fit catalysis is conceptually similar to catalysis via shape complementarity and is worth mentioning here. Geodesic polyarenes are polycyclic aromatic hydrocarbons (PAHs) in which structural geometry constraints result in a curved π-system.[81–84] These systems exhibit unique structural, electronic, and optical properties, such as large dipole moments and dynamic bowl-inversion behavior.[82–89] In the prototypical corannulene molecule ($C_{20}H_{10}$), a pentagon surrounded by five hexagons results in a highly strained bowl-shaped structure with a bowl depth of 0.87 Å. [90] Corannulene undergoes a rapid bowl-to-bowl inversion via a planar transition structure. For example, it is estimated that corannulene inverts more than 200,000 times per second at room temperature.[91] Siegel and co-workers performed DFT calculations and dynamic ^{1}H NMR measurements to show that when corannulene passes through a cyclophane receptor catalyst, the barrier for the bowl inversion in corannulene is significantly reduced relative to the barrier of the uncatalyzed reaction.[92] Following this work, Kroeger and Karton used extensive DFT and energy decomposition analysis calculations to demonstrate that perylene bisimide cyclophanes can catalyze a range of stereo-inversion processes via induced-fit catalysis.[93,94] These processes include the structural inversions of annulenes, bowl-to-bowl inversions of geodesic PAHs and phosphangulenes, and the enantiomerizations of substituted biphenyl and biaryl compounds. More recently,[95] Siegel and co-workers showed that this type of induced-fit catalysis could be inhibited by a transition-state phenanthroline analog. This work demonstrates that a complex catalytic/inhibition enzymatic activity which normally requires an organized array of biological functional groups can be mimicked using a simple abiological system. Similar to enzymatic catalysis,[96] this type of induced-fit catalysis typically involves both ground-state destabilization and transition-state stabilization.[92–95,97]

1.4 Role of Computational Chemistry in Investigating Nanomaterials

Before proceeding to describe the unique catalytic properties of pristine graphene, it is instructive to emphasize the role of computational chemistry in these discoveries. Parallel with the increased experimental research into new catalytic applications of graphene-based materials is the increased computational modeling of their chemical properties. Computational chemistry is a branch of chemistry that models chemical processes by using classical or quantum mechanical calculations rather than experiments. Due to significant advances in quantum chemical theories and high-performance supercomputing technology, computational chemistry provides powerful means for exploring currently unknown chemistry and for designing efficient catalysts and other functional molecules and materials. This approach accelerates the discovery and development of nanomaterials since it is often easier (and cheaper) to investigate a wide range of nanomaterials, chemical processes/properties, and reaction conditions computationally and then synthesize and conduct experiments only for the most promising nanomaterials. Computational modeling is also vital for obtaining mechanistic insights and a better understanding of chemical processes at the molecular and atomic levels.

Nanomaterials, by definition, involve relatively large chemical systems, often with hundreds of atoms or more. Density functional theory is the dominant approach in modeling nanomaterials due to its attractive accuracy-to-computational cost ratio.

DFT calculations scale as N_{bas}^3 for generalized gradient approximation (GGA) methods and as N_{bas}^4 for hybrid-GGA methods, where N_{bas} is the number of basis functions involved in the calculation. For comparison, correlated ab initio calculations scale as N_{bas}^5 (MP2 or DHDFT), N_{bas}^6 (CCSD), and N_{bas}^7 (CCSD(T)).[65,98] In addition, conventional DFT methods (rungs 2–4 of Jacob's Ladder) exhibit a relatively fast basis set convergence relative to correlated ab initio methods such as second-order Møller–Plesset perturbation (MP2), double-hybrid DFT (DHDFT), and coupled-cluster (CC) methods. Therefore, in many DFT investigations, it is often sufficient to optimize the equilibrium and transition structures in conjunction with a double-ζ basis set, such as Def2-SVP, and refine the electronic energies in conjunction with a triple-ζ basis set, such as Def2-TZVP. [99–101] This is due not only to the relatively fast basis-set dependence of DFT methods but also to systematic basis-set errors, which tend to cancel out in the calculation of reaction energies and barrier heights. [102–105] In contrast, correlated ab initio calculations such as MP2, DHDFT, and CCSD(T) require significantly larger basis sets due to their exceedingly slow basis set convergence.[65,98,106] Having said that, some caution is needed in the choice of DFT method and basis set in any given application of DFT methods, as described in more detail below. For additional in-depth discussions, we recommend several recent reviews and perspective articles.[99,107,108]

Due to the computational cost and predictive accuracy of dispersion-corrected DFT methods, DFT simulations have played a critical role over the past decade in (1) the computational and rational design of functional 2D materials, (2) the discovery of new 2D materials, and (3) exploring new functionalities of 2D materials.[58,109–113] Kohn–Sham DFT involves an unknown exchange-correlation (XC) functional, which must be modeled somehow.[114,115] Over the past three decades, there have been extensive theoretical developments of new XC functionals, resulting in numerous different models for the XC functional.[108,116,117] The performance of the various XC approximations can vary significantly for different chemical properties and systems. For example, a DFT method that shows good performance for bond dissociation energies may not show equally good performance for reaction barrier heights. Likewise, a DFT method that performs well for main-group species may not perform well for transition metal systems. Therefore, in practical applications of DFT, it is important to choose a DFT method that gives reliable results for the chemical system and property at hand. There are two straightforward approaches to guide the selection of a suitable DFT method (1) Perdew's Jacob's Ladder of DFT and (2) conducting a literature search for DFT benchmark studies that evaluated the performance of DFT methods for similar chemical systems and properties. The performance of DFT methods has been extensively benchmarked for a wide range of chemical systems and properties. These studies resulted in extensive performance evaluations of many DFT methods covering a wide range of thermochemical and kinetic properties across the Periodic Table.[115–118] In addition, a general concept that helps select an appropriate DFT method is Jacob's Ladder of DFT.[119] Generally speaking, performance for most chemical properties improves with the level of sophistication of the XC functional. That is, performance improves in the order (1) methods employing only the local density; (2) pure GGA methods, which additionally employ the reduced density gradient; (3) meta-GGA methods, which additionally employ the kinetic energy density; (4) hybrid-meta-GGA methods, which additionally involve the occupied orbitals; and (5) DHDFT functionals, which additionally employ the virtual orbitals. For examining catalytic processes, it is desirable to use a DFT method that performs well for both reaction energies and barrier heights.[120] It is well-established that pure GGA methods typically do not perform well for either reaction barrier heights or for challenging thermochemical properties. Therefore, GGA methods are not recommended for investigating catalytic processes.[116,117] Hybrid GGA methods often exhibit a trade-off between their performance for thermochemistry and kinetics, depending on the percentage of Hartree–Fock (HF) exchange incorporated in the functional form.[116,117,121] Functionals with moderate amounts of HF exchange ($\sim$20%) perform well for thermochemistry, whereas functionals with high amounts of HF exchange ($\sim$40%) perform well for reaction barrier heights. Hybrid-meta GGA methods (rung 4 of Jacob's Ladder) and double-hybrid methods (rung 5 of Jacob's Ladder) can overcome this deficiency to a considerable extent.[116,117,121–123] Therefore, it is recommended to use hybrid-meta GGA (and, where possible, DHDFT) methods for investigations of catalytic potential energy surfaces (PESs).

Modeling nanomaterials using molecular orbital DFT often requires using model systems. Nanographenes are often used as models of graphene in hybrid DFT and DHDFT simulations.[46,66,74–79,124–134] This approach allows for the use of more advanced and accurate electronic structure methods than those available (or computationally affordable) in periodic boundary conditions simulations, which are often limited to dispersion-corrected GGA methods. In molecular orbital DFT simulations, one would normally use a nanographene with a diameter ranging between 1 and 3 nm, such as (diameter given in parentheses) $C_{54}H_{18}$ (1.2 nm), $C_{96}H_{24}$ (1.7 nm), $C_{150}H_{30}$ (2.2 nm), and $C_{216}H_{36}$ (2.7 nm). In the following sections, we will focus on the computational studies which predicted that pristine graphene could catalyze chemical processes via π-interactions and shape complementarity.

2 Catalysis by Pristine Graphene

Sections 1.1–1.3 illustrate that both accumulative vdW interactions and shape complementarity can play important roles in chemical catalysis. These aspects have been firmly established as essential parts of chemical catalysis for many years. However, they become particularly important (and sometimes the only means) for stabilizing transition structures with little or no charge separation and directional functional groups (e.g., hydrogen bond donors or acceptors). Pristine graphene is characterized by the following properties:

- The largest surface area of any known material
- Distinct planar two-dimensional morphology
- Evenly distributed π-system across the monolayer
- Can interact with substrates via accumulative van der Waals interactions

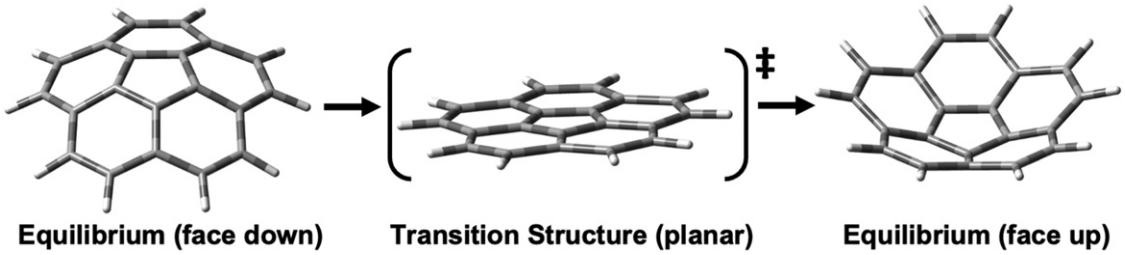

Fig. 2 Equilibrium and transition structures in the bowl-to-bowl inversion in corannulene.

Due to these unique properties, pristine graphene is emerging as an ideal catalyst for chemical processes that proceed via a planar (or nearly planar) transition structure. The availability of a vast 2D π-system is particularly important for this form of catalysis. Here, extensive π-π and σ-π interactions act as the main driving force for catalysis. The magnitude of these interactions is proportional to the size of the substrate and the size of the substrate's π-system. Importantly, catalysis by pristine graphene also overcomes the need for the chemical functionalization of the monolayer. Thus, pristine graphene is a readily available and environmentally sustainable heterogeneous catalyst.

2.1 Pristine Graphene Catalysis of Bowl-to-Bowl Inversion in Geodesic Aromatic Systems

Due to its large surface area and excellent chemical and mechanical stability, pristine graphene has been extensively used as a 2D material for templated synthesis and for 2D assembly of molecules and nanomaterials.[20] In these applications, graphene serves as a growth template for assembling organic systems (such as pentacene[135] and phthalocyanines)[136,137] and inorganic systems (such as gold cyanide nanowires).[138] Here, van der Waals and electrostatic interactions play a key role in the spontaneous assembly of the organic and inorganic substrates on the graphene monolayer. In addition to the applications in templated synthesis and self-assembly, it has been found that pristine graphene (or nano-sized fragments of graphene) can significantly speed up the rate of reactions that proceed via planar (or nearly planar) transition structures.[46,74–79] The first example of this unique catalytic activity has been demonstrated for the inversion reaction of non-planar aromatic compounds such as the fragments of the famous Buckminsterfullerene (C_{60}) carbon cluster. Buckminsterfullerene is a highly symmetrical molecule that can be broken down into two basic geodesic PAH fragments – corannulene and sumanene.[139]

Let us begin with the bowl-to-bowl inversion in corannulene. Corannulene is one of the most interesting PAHs – it involves a pentagon completely surrounded by hexagons, and therefore due to geometrical ring strain, it adopts a bowl-shaped structure. The depth of the bowl has been measured to be $\sim$0.87 Å depending on the temperature.[90,140] Corannulene has 20 π-electrons and is therefore not aromatic according to the Hückel $4n + 2$ rule. However, it still benefits from a significant resonance stabilization energy, which has been estimated to be 186.2 kJ mol^{-1} (cf. a value of 244.3 kJ mol^{-1} obtained for coronene).[141] The planar structure of corannulene is a first-order saddle point corresponding to the bowl-to-bowl inversion. It has been found that increased π-electron delocalization stabilizes the planar structure of corannulene by about 44.8 kJ mol^{-1} relative to the bowl-shaped structure. However, the planar structure also involves a significantly increased level of strain which destabilizes it by about 100.4 kJ mol^{-1} relative to the bowl-shaped structure.[141] These opposite effects result in a planarization barrier of 48.1 kJ mol^{-1} estimated from dynamic ^{1}H NMR measurements.[142,143] **Fig. 2** shows the equilibrium and transition structures involved in the bowl-to-bowl inversion. It is important to note in this context that a single substitution at the rim of the bowl with a simple functional group, such as a halide or a methyl, renders the concave and convex structures to be configurationally stable chiral enantiomers. Finally, one of the most interesting aspects of corannulene is that it has a relatively large dipole moment of 2.07 Debye.[144] This curvature-induced dipole moment is partly attributed to the π-electron flexoelectric effect arising from the polarization of the π bonds in the direction normal to the plane of the central five-membered ring. It has been shown that this relatively large dipole moment plays an important role in self-assembly processes and adsorption at the surface of carbon materials.[145,146]

So far, we have seen the following structural and chemical properties of pristine graphene and corannulene (i) graphene has a distinct 2D planar morphology, (ii) graphene has an extended π-system that interacts with hydrocarbon substrates via cumulative π-π and σ-π interactions, (iii) the bowl-to-bowl inversion in corannulene involves nonplanar reactants and products, but a completely planar transition structure (**Fig. 2**). These observations raise the following hypothesis regarding the interaction between graphene and corannulene: due to shape complementarity, pristine graphene should interact more strongly with the planar bowl-to-bowl inversion transition structure than with the nonplanar bowl-shaped equilibrium structure. This means that pristine graphene would catalyze the bowl-to-bowl inversion in corannulene. This hypothesis was found to be true nearly a decade ago using DHDFT calculations.[74] In particular, these high-level computational simulations predicted that a nanographene catalyst reduces the reaction barrier height for the bowl-to-bowl inversion by about 50%. **Fig. 3** shows the Gibbs free PES for the uncatalyzed bowl-to-bowl inversion in corannulene, calculated at the revDSD-PBEP86-D3BJ/Def2-TZVPP.[101,147,148] We note that this spin-component-scaled DHDFT method has been found that reproduce reaction barrier heights calculated at the CCSD(T)/CBS level of theory within chemical accuracy defined as errors below 4 kJ mol^{-1} for similar reaction barrier heights.[65,74,147–149] Accordingly, there is excellent agreement between the calculated ($\Delta G^{\ddagger}_{298,\mathrm{calc}}$ = 47.3 kJ mol^{-1}) and the experimental value ($\Delta G^{\ddagger}_{298,\mathrm{expt}}$ = 48.1 kJ mol^{-1}).[46] As can be seen in **Fig. 3**, the PES for the bowl-to-bowl inversion in free corannulene is symmetric. However, performing the bowl-to-bowl inversion on a $C_{96}H_{24}$ nanographene results in two dramatic modifications to the PES. First, the PES is no longer symmetric; that is, graphene introduces a thermodynamic drive towards the

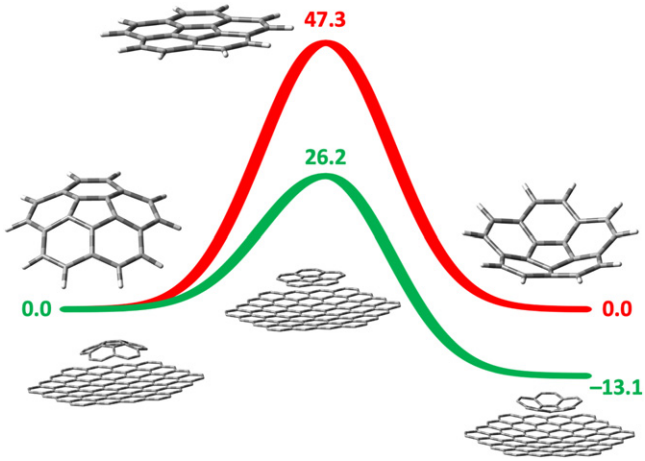

Fig. 3 Schematic Gibbs free potential energy profiles (ΔG_{298}, revDSDPBEP86-D3BJ/Def2-TZVPP, kJ mol^{-1}) for the bowl-to-bowl inversion in free corannulene (red curve) and catalyzed by pristine graphene (green curve). The equilibrium and transition structures and complexes located along the reaction profiles are shown. For further details, see Karton, A., 2020. Catalysis on pristine 2D materials via dispersion and electrostatic interactions. J. Phys. Chem. A 124, 6977–6985.

product in which corannulene is situated face-up on the graphene monolayer. Second, the reaction barrier heights in both directions are significantly reduced relative to the uncatalyzed reaction barrier height of 47.3 kJ mol^{-1}. In particular, we obtain reaction barrier heights of 26.1 and 39.3 kJ mol^{-1} for the forward and reverse reactions, respectively. We note that according to the Eyring equation, a reduction of 5.7 kJ mol^{-1} in the reaction barrier height corresponds to an increase of one order of magnitude in the reaction rate at room temperature. Therefore, the calculated catalytic enhancements ($\Delta\Delta G^{\ddagger}_{298} = \Delta G^{\ddagger}_{298,\mathrm{uncat}} - \Delta G^{\ddagger}_{298,\mathrm{cat}}$) of 21.2 kJ mol^{-1} in the forward direction and 8.0 kJ mol^{-1} in the reverse direction correspond to rate enhancements of 3.7 and 1.4 orders of magnitude, respectively.

These computational results indicate that graphene can not only catalyze the bowl-to-bowl inversion in corannulene but also orient the bowl to be situated face-up on the monolayer. The preferential binding of corannulene in a face-up orientation is due to the larger π-system and electron density on the outside of the bowl compared to the inside of the bowl.[46,145,146,150] We note that this type of directional self-assembly on graphene could result in a hybrid nanocarbon material with unique electronic properties due to the considerable molecular dipole moment of corannulene of 2.07 Debye (cf. with dipole moments of ~1.8 Debye for water and hydrogen fluoride).[144] We hope that these computational predictions will inspire experimental explorations of the graphene-catalyzed bowl-to-bowl inversion in corannulene and the directional self-assembly of corannulene on graphene.

Sumanene is another bowl-shaped fragment of C_{60}.[83,151–153] However, whilst corannulene and sumanene are geometrically similar, they exhibit significant structural differences. First, corannulene is a pentagon surrounded by five pentagons, whereas sumanene is a hexagon surrounded by three pentagons and three hexagons. In addition, corannulene involves only sp^2 carbons, whereas sumanene involves eighteen sp^2 carbons and three sp^3 carbons. In essence, sumanene can be thought of as triphenylene in which the three terminal phenyl rings are connected via sp^3 carbons, forcing a bowl-shaped structure. Sumanene has a deeper bowl, with a depth of 1.11 Å, and accordingly, the reaction barrier for the bowl-to-bowl inversion is considerably higher than in corannulene. At the above level of theory (revDSDPBEP86-D3BJ/Def2-TZVPP), we obtain $\Delta G^{\ddagger}_{298,\mathrm{calc}} = 85.0$ kJ mol^{-1} for the bowl-to-bowl inversion in sumanene (**Fig. 4**). As is the case for the bowl-to-bowl inversion in corannulene, the calculated reaction barrier height is in excellent agreement with the experimental reaction barrier height of $\Delta G^{\ddagger}_{303,\mathrm{expt}} = 84.9$ kJ mol^{-1}, obtained from 2D NMR measurements.[154]

A nanographene catalyst affects the PES for the bowl-to-bowl inversion in sumanene in a similar way to the bowl-to-bowl inversion in corannulene. However, an important distinction is that the thermodynamic driving force for the sumanene bowl being situated face-up on the graphene monolayer becomes significantly larger. Namely, the thermodynamic preference for the bowl facing upwards increases from 13.1 kJ mol^{-1} in corannulene (**Fig. 3**) to 34.1 kJ mol^{-1} in sumanene (**Fig. 4**). Overall, the nanographene catalyst reduces the reaction barrier for the bowl-to-bowl inversion in sumanene from 85.0 kJ mol^{-1} in the uncatalyzed inversion to 39.2 kJ mol^{-1} in the forward direction and to $\Delta G^{\ddagger}_{298,\mathrm{calc}} = 73.3$ kJ mol^{-1} in the reverse direction. The relatively low reaction barrier height in the forward direction indicates that it should be possible to orient sumanene molecules adsorbed on graphene with their bowls facing upwards. The relatively high barrier in the reverse direction indicates that this directional self-assembly on graphene could remain stable at temperatures around 273 K. This makes sumanene a more suitable candidate than corannulene for directional self-assembly on graphene. In this context, it should be mentioned that sumanene has a similar diploe moment to that of corannulene and that the three benzylic CH_2 groups offer functionalization routes that are not possible in corannulene.[153] Again, we hope that these computational predictions will inspire experimental explorations of the catalyzed bowl-to-bowl inversion and directional self-assembly of sumanene on single-layer graphene.

The catalytic enhancements in the graphene-catalyzed bowl-to-bowl inversions in corannulene and sumanene are driven by shape complementarity between planar graphene and planar transition structure, enabling greater stabilization of the transition structures over the bowl-shaped equilibrium structures. At the revDSD-PBEP86-D3BJ/Def2-TZVPP level of theory, the interaction

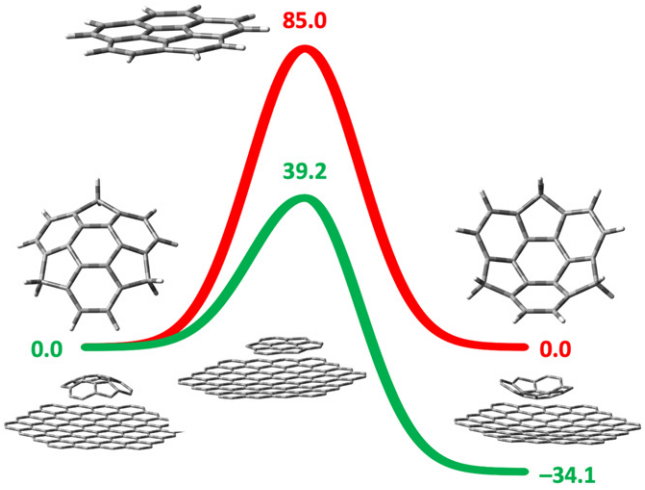

Fig. 4 Schematic Gibbs free potential energy profiles (ΔG_{298}, revDSDPBEP86-D3BJ/Def2-TZVPP, kJ mol^{-1}) for the bowl-to-bowl inversion in free sumanene (red curve) and catalyzed by pristine graphene (green curve). The equilibrium and transition structures and complexes located along the reaction profiles are shown. For further details, see Karton, A., 2020. Catalysis on pristine 2D materials via dispersion and electrostatic interactions. J. Phys. Chem. A 124, 6977–6985.

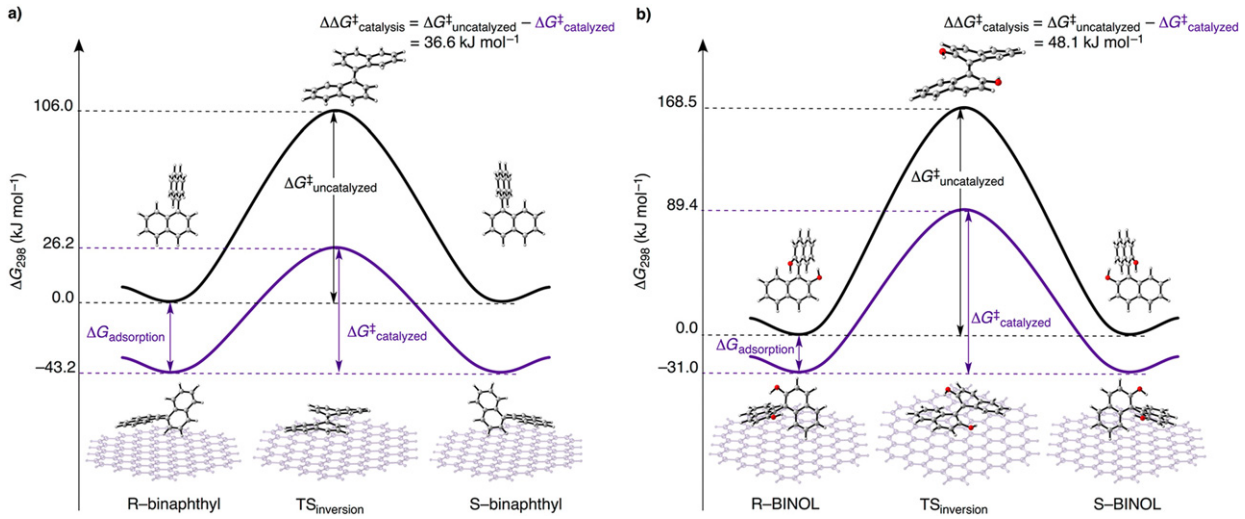

Fig. 5 Schematic potential energy profiles for the uncatalyzed and graphene-catalyzed enantiomerizations of (a) 1,1'-binaphthyl and (b) BINOL. The Gibbs free activation energies at 298K are calculated at the PW6B95-D3BJ/Def2-TZVPP level of theory and are given in kJ mol^{-1}. Figure reprinted with permission from Kroeger, A.A., Karton, A., 2019. Catalysis by pure graphene—From supporting actor to protagonist through shape complementarity. J. Org. Chem. 84, 11343–11347.

energy between the nanographene catalyst and corannulene amounts to 174.1 kJ mol^{-1} in the complex where the bowl is faced downwards (reactant in **Fig. 3**) and 187.2 kJ mol^{-1} in the complex where the bowl is faced upwards (product in **Fig. 3**). However, the interaction energy increases to 195.2 kJ mol^{-1} in the transition structure complex where there is more effective overlap between the π-systems of corannulene and the nanographene catalyst due to shape complementarity. It is also instructive to shed light on the intermolecular forces responsible for this catalytic activity via energy decomposition analyses,[155,156] which show that the 2D graphene sheet stabilizes the planar transition structure via dispersion and electrostatic interactions. Very similar observations are made for the bowl-to-bowl inversion in sumanene, see Ref. 46 for further details.

2.2 Pristine Graphene Catalyzed Enantiomerization of Biphenyls and Biaryls of Synthetic Relevance

We have shown above that nanographene can efficiently catalyze the bowl-to-bowl inversion in corannulene and sumanene through shape complementarity and π-π interactions. Over the past decade, it has been found that pristine graphene can also efficiently catalyze rotation processes involving biphenyls and biaryls.[46,74,76,77] These findings are exciting not only because they

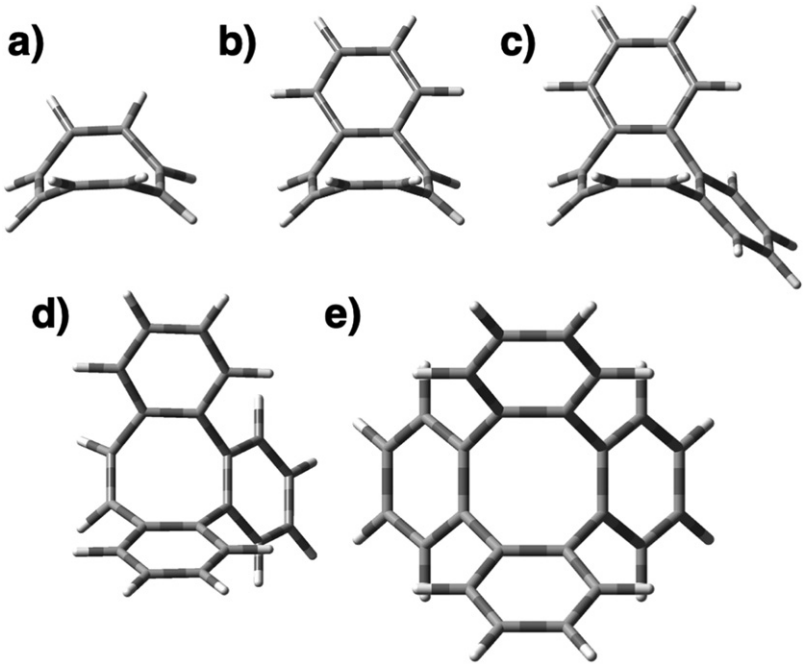

Fig. 6 Equilibrium structures of a series of benzannulated COT derivatives with an increasing level of benzannulation in adjacent positions (a) COT, (b) mono-benzannulated COT, (c) di-benzannulated COT, (d) tri-benzannulated COT, and (e) tetra-benzannulated COT. The DFT-optimized structures are taken from Kroeger, A.A., Karton, A., 2021. π-π catalysis in carbon flatland—flipping [8]annulene on graphene. Chem. Eur. J. 27, 3420–3426.

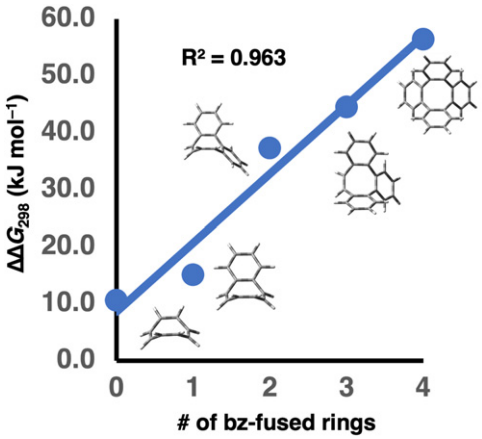

Fig. 7 Catalytic enhancements ($\Delta\Delta G^{\ddagger}_{298}$) for the graphene-catalyzed skeletal inversions of a series of benzannulated COT derivatives. These results are taken from reference Kroeger, A.A., Karton, A., 2021. π-π catalysis in carbon flatland—flipping [8]annulene on graphene. Chem. Eur. J. 27, 3420–3426.

generalize the catalytic activity of pristine graphene but also because they extend pristine 2D catalysis to processes of synthetic relevance, such as the dynamic kinetic resolution of biaryls. [157–160]

Let us begin with the rotation about the C–C bond in biaryls. 1,1′-binaphthyl is composed of two naphthyl units linked by a sigma C–C bond. Due to steric repulsions, 1,1′-binaphthyl is a highly nonplanar aromatic compound with a torsional angle of 68.6° between the two naphthyl units.[76] 1,1′-binaphthyl has axial chirality and can exist as two configurationally stable enantiomers. The interconversion between the two enantiomers can proceed via a syn- or anti-type transition structure. The anti-type transition structure is kinetically favorable. The reaction barrier for the rotation about the C–C bond has been calculated at the PW6B95-D3BJ/Def2-TZVPP level of theory to be 106.0 kJ mol^{-1}. [161] This reaction barrier height is in good agreement with the experimentally available reaction barrier heights of 98.5 and 100.7 kJ mol^{-1}.[162,163] **Fig. 5**(a) compares the reaction profiles on the Gibbs free PES for the uncatalyzed and graphene-catalyzed chirality inversions. As can be seen in the uncatalyzed reaction profile, the naphthyl units in the transition structure are nearly co-planar (**Fig. 5**(a)). Therefore, it is expected that pristine graphene would catalyze the chirality inversion. Indeed, a nanographene catalyst reduces the calculated reaction barrier height by as much as 36.6 kJ mol^{-1} resulting in a

catalytic barrier height of 69.4 kJ mol^{-1}. Inspection of the graphene-catalyzed reaction profile in **Fig. 5**(a) reveals that in the equilibrium complex, only one naphthyl unit is parallel to the graphene catalyst due to the large torsional angle between the two naphthyl units. The complexation energy in this equilibrium complex amounts to 43.2 kJ mol^{-1}. However, in the transition structure complex, where both the 1,1′-binaphthyl and graphene are nearly planar, both naphthyl units lie parallel to the graphene catalyst, resulting in a more effective overlap between the two π-systems. The more effective overlap between the two π-systems in the transition structure complex relative to the equilibrium complex is the origin of the relatively large catalytic enhancement of $\Delta\Delta G^{\ddagger}_{298} = 36.6$ kJ mol^{-1} (**Fig. 5**(a)).

Let us move to the graphene-catalyzed rotation of the C–C bond in 1,1′-binaphthyl-2,2′-diol (BINOL). BINOL is a highly privileged axially chiral scaffold, which forms the basis for many chiral organometallic catalysts, as well as the starting material in the synthesis of a growing family of phosphoric acid organocatalysts. [164–166] However, the enantioselective production of BINOL and its derivatives remains a challenge. Kinetic resolution strategies are often generally applicable and suited to large-scale synthesis but suffer from the inherent limitations of waste and separation, as the yield is limited to a maximum of 50%. Therefore, dynamic kinetic resolution forms an attractive synthesis strategy.[157,167,168] In 2018, Akai utilized a ruthenium-based catalyst for the racemization of BINOL, which was combined with a lipase-catalyzed acylation for the dynamic kinetic resolution of BINOL.[157] Pristine graphene may serve as an environmentally benign and economical alternative to the homogeneous ruthenium catalyst. The above results for 1,1′-binaphthyl suggest that pristine graphene could efficiently catalyze the racemization of axially chiral, configurationally stable BINOL. **Fig. 5**(b) shows the uncatalyzed and graphene-catalyzed enantiomerization of BINOL. The reaction barrier height for the uncatalyzed racemization amounts to 168.5 kJ mol^{-1}. Accordingly, the uncatalyzed process requires temperatures above 200°C. [169,170] A nanographene catalyst results in an appreciable catalytic enhancement of $\Delta\Delta G^{\ddagger}_{298} = 48.1$ kJ mol^{-1} (**Fig. 5**(b)). Inspection of **Fig. 5**(b), reveals that the graphene-catalyzed racemization of 1,1′-binaphthyl and BINOL involve similar equilibrium and transition structure complexes. We note that similar to the bowl-to-bowl inversion in corannulene and sumanene, this catalytic activity is driven by dispersion and electrostatic interactions.[77] Following the above computational results for the graphene-catalyzed racemization of BINOL, this computational prediction has been confirmed experimentally through chiral HPLC measurements.[77] In particular, it was found experimentally that a single-layer graphene sheet efficiently catalyzes the BINOL racemization, with near-complete racemization after 24 h at 60°C.

Finally, we note that it has been demonstrated computationally that graphene can also catalyze the rotation about the C–C bond in biphenyl and substituted biphenyls. Biphenyl is a nonplanar aromatic compound in which steric repulsion between the hydrogens in the ortho positions results in a torsional angle between the two phenyl rings. For example, in unsubstituted biphenyl, the equilibrium torsional angle is 44.4°.[171] The structure in which the torsional angle is 0° is a first-order saddle point corresponding to the rotation about the C–C bond. Thus, the rotation about the C–C bond in biphenyls involves nonplanar reactants/products and completely planar transition structures. Using DHDFT calculation, it was found that a nanographene can catalyze these rotation processes in the same manner as the biaryl racemizations.[46,74]

2.3 Pristine Graphene Catalyzed Skeletal Inversions of Helicenes and Cyclooctatetraene Derivatives

As a final example, we consider skeletal inversions in two types of polycyclic hydrocarbons – benzannulated cyclooctatetraenes and helicenes. Let us begin with the ring inversions of the 1,3,5,7-cyclooctatetraene (COT) skeleton. Cyclooctatetraene is the smallest nonplanar annulene, which adopts a tub shape structure to avoid antiaromaticity. This unique scaffold makes benzanulated COT derivatives versatile ligands in enantioselective catalysis.[172–174] Here, we are interested in the series of benzannulated COT derivatives with an increasing level of benzannulations in neighboring positions as shown in **Fig. 6**. This series of compounds has attracted significant theoretical and experimental attention.[175–179] The tub-to-tub inversion in COT and mono-benzannulated COT proceeds via completely planar transition structures. Due to steric repulsion between the adjacent benzene rings, however, the tub-to-tub inversions in di-, tri-, and tetra-benzanulated COT proceed via nonplanar propeller-shaped transition structures. This set of skeletal inversions provides a series of increasing barrier heights. For example, at the PW6B95-D3BJ/Def2-TZVPP level of theory, the following barrier heights are obtained for the uncatalyzed inversions 50.1 (mono-benzanulated COT), 126.3 (di-benzannulated COT), 171.6 (tri-benzanulated COT), and 322.0 (tetra-benzanulated COT) kJ mol^{-1}. It is interesting to examine the graphene catalysis of these tub-to-tub inversions since they involve highly nonplanar equilibrium structures, but transition structures that are either completely planar (COT and mono-benzannulated COT) or significantly more planar than the corresponding equilibrium structures (di-, tri-, and tetra-benzannulated COT).[78] It should be pointed out that the reaction barrier height for the tub-to-tub inversion in tetrabenzanulated COT is so high that it will decompose upon heating before this large barrier can be surmounted.[179] Therefore, a catalyst is essential for this skeletal inversion.

It has been shown computationally that a pristine graphene catalyst can efficiently catalyze the skeletal inversions of COT and the four benzannulated COT derivatives in **Fig. 6**. This is another example of a pristine-graphene-catalyzed process solely driven by shape complementarity and π-stacking interactions.[78] In particular, at the PW6B95-D3BJ/Def2-TZVPP level of theory, the uncatalyzed barrier heights (vide supra) are reduced by 10.6 (COT), 15.1 (monobenzanulated COT), 37.3 (dibenzannulated COT), 44.5 (tribenzanulated COT), and 56.4 (tetrabenzanulated COT) kJ mol^{-1}. These catalytic enhancements correspond to barrier reductions by 17.5–30.2% relative to the uncatalyzed reaction barrier heights. We note that according to the Eyring equation, these catalytic enhancements translate to increases of 2–10 orders of magnitude in the reaction rate at room temperature.

The graphene-catalyzed skeletal inversions of the benzannulated COT derivatives in **Fig. 6** allow us to examine the catalytic enhancements for a systematic series of benzanulated COT derivatives of increasing size and reaction barrier heights. **Fig. 7** depicts the catalytic enhancements ($\Delta\Delta G^{\ddagger}_{298} = \Delta G^{\ddagger}_{298,\mathrm{uncat}} - \Delta G^{\ddagger}_{298,\mathrm{cat}}$) for the series of benzannulated COT derivatives. It is evident that

these catalytic enhancements increase linearly with the number of benzannulations, indicating that the transition structure stabilization increases with the size of the system.

Finally, we note that a similar type of skeletal inversion – the 'flip-flop' inversion in helicenes – has also been found to be catalyzed by a nanographene.[74] In particular, the smallest helicene (benzo[*c*]phenanthrene) has a nonplanar equilibrium structure due to steric repulsion between the hydrogens on the terminal phenyl rings.[180–182] Therefore, benzo[*c*]phenanthrene oscillates rapidly between two chiral helical conformations via a completely planar transition structure. Even though the calculated reaction barrier height is very low and amounts to 17.9 kJ mol^{-1}, a small coronene catalyst is still able to reduce it by about 20%,[74] and it is expected that a larger nanographene would result in a larger catalytic enhancement. A question that remains unanswered is whether graphene would be able to catalyze the 'flip-flop' inversion in larger helicenes.

3 Conclusions

Pristine graphene is characterized by a large surface area, a planar two-dimensional morphology, and an evenly distributed π-system across the monolayer. These unique properties make pristine graphene an ideal catalyst for a range of chemical processes. This chapter summarizes recent computational (and some experimental) advances in this exciting emerging form of catalysis by pristine graphene. These theoretical and experimental results pave the way for developing sustainable and environmentally benign 2D graphene catalysts that are readily available and require no chemical modification or functionalization. In particular, based on extensive computational DFT simulations, it has been predicted that pristine graphene can efficiently catalyze the following chemical processes:

- Bowl-to-bowl inversion of curved aromatic molecules (e.g., corannulene and sumanene)
- Enantiomerizations of substituted biphenyl and biaryl compounds (e.g., 2,2′-dimethyl-biphenyl; 1,1′-binaphthyl; and BINOL),
- Skeletal inversions of helicenes (e.g., benzo[*c*]phenanthrene) and ortho-benzannulated cyclooctatetraene derivatives

Overall, a pristine graphene catalyst accelerates the rates of these reactions by several orders of magnitude. These catalytic enhancements are achieved through shape complementarity between the planar graphene and planar transition structure, enabling disproportionate stabilization of the transition structures relative to the non-planar reactants and products. DFT-based energy decomposition analyses show that this catalytic activity is mainly driven by dispersion and electrostatic forces. The inclusion of aromatic rings in the substrate can dramatically enhance the catalytic enhancement. However, aromatic rings are not strictly necessary for this form of catalysis to proceed. For example, a pristine graphene catalyst reduces the reaction barrier height for the tub-to-tub inversion in unsubstituted cyclooctatetraene by about 20%, even though cyclooctatetraene has a nonaromatic equilibrium structure and an antiaromatic transition structure.

Importantly, the graphene-catalyzed enantiomerization of BINOL has been confirmed experimentally through chiral HPLC measurements shortly after the computational prediction has been made.[76,77] The catalysis of this enantiomerization reaction plays a key role in the synthesis of a wide range of biaryls from a BINOL precursor via dynamic kinetic resolution. This enantiomerization has been catalyzed by a homogeneous ruthenium catalyst in a recent dynamic kinetic resolution application. Thus, the catalytic enantiomerization of BINOL is an example where an organometallic catalyst could be replaced by an environmentally sustainable pristine graphene catalyst in a dynamic kinetic resolution application.

We also review the computational predictions that pristine graphene would catalyze the bowl-to-bowl inversions in orannulene and sumanene through shape complementarity and π-π interactions. The results show not only that a pristine graphene catalyst leads to significant catalytic enhancements of these bowl-to-bowl inversions, but also leads to a thermodynamic drive for directional self-assembly of the bowl situated face-up on the graphene monolayer. This directional self-assembly leads to a hybrid nanocarbon material with unique electronic properties due to the considerable dipole moments of corannulene and sumanene. We hope that these computational predictions will inspire experimental explorations of the graphene-catalyzed bowl-to-bowl inversion in corannulene and sumanene and the directional self-assembly of these bowl-shaped structures on across the graphene monolayer.

Finally, it should be noted that catalysis by pristine graphene paves the way for catalysis by other pristine 2D materials. To this end, it has been recently found, using extensive DHDFT calculations, that the bowl-to-bowl inversion in corannulene and sumanene can be catalyzed by 2D materials with significantly different electronic structures and chemical compositions than graphene – namely inorganic hexagonal boron-nitride (h-BN) and aliphatic graphane.[46]

References

1. Kroto, H.W., Heath, J.R., O'Brien, S.C., Curl, R.F., Smalley, R.E., 1985. C_{60}: Buckminsterfullerene. Nature 318, 162–163.
2. Lu, X., Chen, X., 2005. Curved Pi-conjugation, aromaticity, and the related chemistry of small fullerenes (< C60) and single-walled carbon nanotubes. Chem. Rev. 105, 3643–3696.
3. Iijima, S., 1991. Helical microtubules of graphitic carbon. Nature 354, 56–58.
4. De Volder, M.F.L., Tawfick, S.H., Baughman, R.H., Hart, A.J., 2013. Carbon nanotubes: Present and future commercial applications. Science 339, 535–539.
5. Novoselov, K.S., Geim, A.K., Morozov, S.V., *et al.*, 2004. Electric field effect in atomically thin carbon films. Science 306, 666–669.
6. Novoselov, K.S., Geim, A.K., Morozov, S.V., *et al.*, 2005. Two-dimensional gas of massless Dirac fermions in graphene. Nature 438, 197–200.
7. Novoselov, K.S., Jiang, D., Schedin, F., *et al.*, 2005. Two-dimensional atomic crystals. Proc. Natl Acad. Sci. USA 102, 10451–10453.

8. Allen, M.J., Tung, V.C., Kaner, R.B., 2010. Honeycomb carbon: A review of graphene. Chem. Rev. 110, 132–145.
9. Chen, D., Tang, L.H., Li, J.H., 2010. Graphene-based materials in electrochemistry. Chem. Soc. Rev. 39, 3157–3180.
10. Machado, B.F., Serp, P., 2012. Graphene-based materials for catalysis. Catal. Sci. Technol. 2, 54–75.
11. Xiang, Q., Yu, J., Jaroniec, M., 2012. Graphene-based semiconductor photocatalysts. Chem. Soc. Rev. 41, 782–796.
12. Brownson, D.A.C., Kampouris, D.K., Banks, C.E., 2012. Graphene electrochemistry: Fundamental concepts through to prominent applications. Chem. Soc. Rev. 41, 6944–6976.
13. Wang, H., Dai, H., 2013. Strongly coupled inorganic–nano-carbon hybrid materials for energy storage. Chem. Soc. Rev. 42, 3088–3113.
14. Su, D.S., Perathoner, S., Centi, G., 2013. Nanocarbons for the development of advanced catalysts. Chem. Rev. 113, 5782–5816.
15. Fan, X., Zhang, G., Zhang, F., 2015. Multiple roles of graphene in heterogeneous catalysis. Chem. Soc. Rev. 44, 3023–3035.
16. Deng, D., Fu, Q., Bao, X., *et al.*, 2016. Catalysis with two-dimensional materials and their heterostructures. Nat. Nanotechnol. 11, 218–230.
17. Hu, M., Yao, Z., Wang, X., 2017. Graphene-based nanomaterials for catalysis. Ind. Eng. Chem. Res. 56, 3477–3502.
18. Georgakilas, V., Perman, J.A., Tucek, J., Zboril, R., 2015. Broad family of carbon nanoallotropes: Classification, chemistry, and applications of fullerenes, carbon dots, nanotubes, graphene, nanodiamonds, and combined superstructures. Chem. Rev. 115, 4744–4822.
19. Georgakilas, V., Tiwari, J.N., Kemp, K.C., *et al.*, 2016. Noncovalent functionalization of graphene and graphene oxide for energy materials, biosensing, catalytic, and biomedical applications. Chem. Rev. 116, 5464–5519.
20. Quan, Q., Lin, X., Zhanga, N., Xu, Y.-J., 2017. Graphene and its derivatives as versatile templates ⊘for materials synthesis and functional applications. Nanoscale 9, 2398–2416.
21. Bottari, G., Herranz, M.Á., Wibmer, L., *et al.*, 2017. Chemical functionalization and characterization of graphene-based materials. Chem. Soc. Rev. 46, 4464–4500.
22. Clancy, A.J., Bayazit, M.K., Hodge, S.A., *et al.*, 2018. Charged carbon nanomaterials: Redox chemistries of fullerenes, carbon nanotubes, and graphenes. Chem. Rev. 118 (16), 7363–7408.
23. Nekoueian, K., Amiri, M., Sillanpää, M., *et al.*, 2019. Carbon-based quantum particles: An electroanalytical and biomedical perspective. Chem. Soc. Rev. 48, 4281–4316.
24. Panwar, N., Soehartono, A.M., Chan, K.K., *et al.*, 2019. Nanocarbons for biology and medicine: Sensing, imaging, and drug delivery. Chem. Rev. 119, 9559–9656.
25. Hu, C., Paul, R., Dai, Q., Dai, L., 2021. Carbon-based metal-free electrocatalysts: From oxygen reduction to multifunctional electrocatalysis. Chem. Soc. Rev. 50, 11785–11843.
26. Wu, Y., Zhao, X., Shang, Y., *et al.*, 2021. Application-driven carbon nanotube functional materials. ACS Nano 15, 7946–7974.
27. Binzel, D.W., Li, X., Burns, N., *et al.*, 2021. Promising graphene-based nanomaterials and their biomedical applications and potential risks: A comprehensive review. Chem. Rev. 121, 7398–7467.
28. Georgakilas, V., Otyepka, M., Bourlinos, A.B., *et al.*, 2012. Functionalization of graphene: Covalent and non-covalent approaches, derivatives and applications. Chem. Rev. 112, 6156–6214.
29. Liu, M.M., Zhang, R.Z., Chen, W., 2014. Graphene-supported nanoelectrocatalysts for fuel cells: Synthesis, properties, and applications. Chem. Rev. 114, 5117–5160.
30. Navalon, S., Dhakshinamoorthy, A., Alvaro, M., Garcia, H., 2014. Carbocatalysis by graphene-based materials. Chem. Rev. 114, 6179–6212.
31. Navalon, S., Dhakshinamoorthy, A., Alvaro, M., Antonietti, M., García, H., 2017. Active sites on graphene-based materials as metal-free catalysts. Chem. Soc. Rev. 46, 4501–4529.
32. Wang, Y., Mao, J., Meng, X., *et al.*, 2019. Catalysis with two-dimensional materials confining single atoms: Concept, design, and applications. Chem. Rev. 119, 1806–1854.
33. Konwar, L.J., Mäki-Arvela, P., Mikkola, J.P., 2019. SO_3H-containing functional carbon materials: Synthesis, structure, and acid catalysis. Chem. Rev. 119, 11576–11630.
34. Sun, Z., Fang, S., Hu, Y.H., 2020. 3D graphene materials: From understanding to design and synthesis control. Chem. Rev. 120, 10336–10453.
35. Zhuo, H.-Y., Zhang, X., Liang, J.-X., *et al.*, 2020. Theoretical understandings of graphene-based metal single-atom catalysts: Stability and catalytic performance. Chem. Rev. 120, 12315–12341.
36. Astruc, D., 2020. Introduction: Nanoparticles in catalysis. Chem. Rev. 120, 461–463.
37. Chen, B.W.J., Xu, L., Mavrikakis, M., 2021. Computational methods in heterogeneous catalysis. Chem. Rev. 121, 1007–1048.
38. Khine, Y.Y., Wen, X., Jin, X., Foller, T., Joshi, R., 2022. Functional groups in graphene oxide. Phys. Chem. Chem. Phys. 24, 26337–26355.
39. Sajjad, S., Leghari, S.A.K., Iqbal, A., 2017. Study of graphene oxide structural features for catalytic, antibacterial, gas sensing, and metals decontamination environmental applications. ACS Appl. Mater. Interfaces 9, 43393–43414.
40. Su, C., Loh, P., 2013. Carbocatalysts: Graphene oxide and its derivatives. Acc. Chem. Res. 46, 2275–2285.
41. Pyun, J., 2011. Graphene oxide as catalyst: Application of carbon materials beyond nanotechnology. Angew. Chem. 50, 46–48.
42. Haag, D.R., Kung, H.H., 2014. Metal-free graphene based catalysts: A review. Top. Catal. 57, 762–773.
43. Zhu, S., Wang, J., Fan, W., 2015. Graphene-based catalysis for biomass conversion. Catal. Sci. Technol. 5, 3845–3858.
44. Schaetz, A., Zeltner, M., Stark, W.J., 2012. Carbon modifications and surfaces for catalytic organic transformations. ACS Catal. 2, 1267–1284.
45. Daelemans, B., Bilbao, N., Dehaen, W., De Feyter, S., 2021. Carbocatalysis with pristine graphite: On-surface nanochemistry assists solution-based catalysis. Chem. Soc. Rev. 50, 2280–2296.
46. Karton, A., 2020. Catalysis on pristine 2D materials via dispersion and electrostatic interactions. J. Phys. Chem. A 124, 6977–6985.
47. Hobza, P., Müller-Dethlefs, K., 2009. Noncovalent Interactions. Theory and Experiment, first ed. Cambridge: The Royal Society of Chemistry.
48. Schneider, H.J., 2009. Binding mechanisms in supramolecular complexes. Angew. Chem. Int. Ed. 48, 3924–3977.
49. Gobre, V.V., Tkatchenko, A., 2013. Scaling laws for van der Waals interactions in nanostructured materials. Nat. Commun. 4, 2341.
50. Erbas-Cakmak, S., Leigh, D.A., McTernan, C.T., Nussbaumer, A.L., 2015. Artificial molecular machines. Chem. Rev. 115, 10081–10206.
51. Krenske, E.H., Houk, K.N., 2013. Aromatic interactions as control elements in stereoselective organic reactions. Acc. Chem. Res. 46, 979–989.
52. Wagner, J.P., Schreiner, P.R., 2015. London dispersion in molecular chemistry–reconsidering steric effects. Angew. Chem. Int. Ed. 54, 12274–12296.
53. Wheeler, S.E., Seguin, T.J., Guan, Y., Doney, A.C., 2016. Noncovalent interactions in organocatalysis and the prospect of computational catalyst design. Acc. Chem. Res. 49, 1061–1069.
54. Neel, A.J., Hilton, M.J., Sigman, M.S., Toste, F.D., 2017. Exploiting non-covalent π interactions for catalyst design. Nature 543, 637–646.
55. Davis, H.J., Phipps, R.J., 2017. Harnessing non-covalent interactions to exert control over regioselectivity and site-selectivity in catalytic reactions. Chem. Sci. 8, 864–877.
56. Toste, F.D., Sigman, M.S., Miller, S.J., 2017. Pursuit of noncovalent interactions for strategic site-selective catalysis. Acc. Chem. Res. 50, 609–615.
57. Reid, J.P., Sigman, M.S., 2018. Comparing quantitative prediction methods for the discovery of small-molecule chiral catalysts. Nat. Rev. Chem. 2, 290–305.
58. Su, G., Yang, S., Jiang, Y., *et al.*, 2019. Modeling chemical reactions on surfaces: the roles of chemical bonding and van der Waals interactions. Prog. Surf. Sci. 94, 100561.
59. Acocella, M.R., Mauro, M., Falivene, L., Cavallo, L., Guerra, G., 2014. Inverting the diastereoselectivity of the Mukaiyama – Michael addition with graphite-based catalysts. ACS Catal. 4, 492–496.
60. Acocella, M.R., Maggio, M., Ambrosio, C., Aprea, N., Guerra, G., 2017. Oxidized carbon black as an activator of transesterification reactions under solvent-free conditions. ACS Omega 2, 7862–7867.
61. Liu, Z.-X., Yang, L., Chen, Y.-G., Tian, Z.-Y., Yang, Z.-Y., 2022. Noncovalent wedging effect catalyzed the cis to syn transformation of a surface-adsorbed polymer backbone toward an unusual thermodynamically stable supramolecular product. Phys. Chem. Chem. Phys. 24, 30010–30016.

62. Karton, A., Martin, J.M.L., 2021. Prototypical π-π dimers re-examined by means of high-level CCSDT(Q) composite ab initio methods. J. Chem. Phys. 154, 124117.
63. Janowski, T., Pulay, P., 2012. A benchmark comparison of σ/σ and π/π dispersion: The dimers of naphthalene and decalin, and coronene and perhydrocoronene. J. Am. Chem. Soc. 134, 17520–17525.
64. Janowski, T., Ford, A.R., Pulay, P., 2010. Accurate correlated calculation of the intermolecular potential surface in the coronene dimer. Mol. Phys. 108, 249–257.
65. Karton, A., 2022. Quantum mechanical thermochemical predictions 100 years after the Schrodinger equation. Annu. Rep. Comput. Chem. 18, 123–166.
66. Karton, A., 2022. π-π interactions between benzene and graphene by means of large-scale DFT-D4 calculations. Chem. Phys. 561, 111606.
67. Janowski, T., Pulay, P., 2011. A benchmark quantum chemical study of the stacking interaction between larger polycondensed aromatic hydrocarbons. Theor. Chem. Acc. 130, 419–427.
68. Pauling, L., 1948. Nature of forces between large molecules of biological interest. Nature 161, 707–709.
69. Jencks, W.P., 1969. Catalysis in Chemistry and Enzymology. New York: McGraw-Hill.
70. Xu, J., Deng, Q., Chen, J., *et al*., 1999. Evolution of shape complementarity and catalytic efficiency from a primordial antibody template. Science 286, 2345–2348.
71. Chen, J., Deng, Q., Wang, R., Houk, K.N., Hilvert, D., 2000. Shape complementarity, binding-site dynamics, and transition state stabilization: A Theoretical study of Diels-Alder catalysis by antibody 1E9. ChemBioChem 1, 255–261.
72. Hugot, M., Bensel, N., Vogel, M., *et al*., 2002. A structural basis for the activity of retro-Diels-Alder catalytic antibodies: Evidence for a catalytic aromatic residue. Proc. Natl Acad. Sci. USA 99, 9674–9678.
73. Amyes, T.L., Richard, J.P., 2013. Specificity in transition state binding: The Pauling model revisited. Biochemistry 52, 2021–2035.
74. Karton, A., 2014. Inversion and rotation processes involving non-planar aromatic compounds catalyzed by extended polycyclic aromatic hydrocarbons. Chem. Phys. Lett. 614, 156–161.
75. Denis, P.A., 2015. Pristine graphene-based catalysis: Significant reduction of the inversion barriers of adsorbed and confined corannulene, sumanene, and dibenzo[a,g] corannulene. J. Phys. Chem. A 119, 5770–5777.
76. Kroeger, A.A., Karton, A., 2019. Catalysis by pure graphene—From supporting actor to protagonist through shape complementarity. J. Org. Chem. 84, 11343–11347.
77. Kroeger, A.A., Hooper, J.F., Karton, A., 2020. Pristine graphene as a racemization catalyst for axially chiral BINOL. ChemPhysChem 21, 1675–1681.
78. Kroeger, A.A., Karton, A., 2021. π-π catalysis in carbon flatland—flipping [8]annulene on graphene. Chem. Eur. J. 27, 3420–3426.
79. Denis, P.A., 2022. Helicene adsorption on graphene, hexagonal boron nitride, graphane, and fluorographene. Chem. Phys. Lett. 806, 139998.
80. Hilvert, D., Hill, K.W., Nared, K.D., Auditor, M.T.M., 1989. Antibody catalysis of the Diels-Alder reaction. J. Am. Chem. Soc. 111, 9261–9262.
81. Scott, L.T., Petrukhina, M., 2011. Fragments of Fullerenes and Carbon Nanotubes: Designed Synthesis, Unusual Reactions, and Coordination Chemistry. John Wiley & Sons.
82. Tsefrikas, V.M., Scott, L.T., 2006. Geodesic Polyarenes by flash vacuum pyrolysis. Chem. Rev. 106, 4868–4884.
83. Wu, Y.-T., Siegel, J.S., 2006. Aromatic molecular-bowl hydrocarbons: Synthetic derivatives, their structures, and physical properties. Chem. Rev. 106, 4843–4867.
84. Rabideau, P.W., Sygula, A., 1996. Buckybowls: Polynuclear aromatic hydrocarbons related to the buckminsterfullerene surface. Acc. Chem. Res. 29, 235–242.
85. Saito, M., Shinokubo, H., Sakurai, H., 2018. Figuration of bowl-shaped p-conjugated molecules: Properties and functions. Mater. Chem. Front. 2, 635–661.
86. Wu, Y.-T., Siegel, J.S., 2014. Synthesis, structures, and physical properties of aromatic molecular-bowl hydrocarbons. Top. Curr. Chem. 349, 63–120.
87. Sygula, A., 2011. Chemistry on a half-shell: Synthesis and derivatization of buckybowls. Eur. J. Org. Chem. 2011, 1611–1625.
88. Higashibayashi, S., Sakurai, H., 2011. Synthesis of sumanene and related buckybowls. Chem. Lett. 40, 122–128.
89. Petrukhina, M.A., Scott, L.T., 2005. Coordination chemistry of buckybowls: From corannulene to a hemifullerene. Dalton Trans. 2969–2975.
90. Hanson, J.C., Nordman, C.E., 1976. The crystal and molecular structure of corarmulene, $C_{20}H_{10}$. Acta Crystallogr. B B32, 1147–1153.
91. Scott, L.T., Hashemi, M.M., Bratcher, M.S., 1992. Corannulene bowl-to-bowl inversion is rapid at room temperature. J. Am. Chem. Soc. 114, 1920–1921.
92. Jurícek, M., Strutt, N.L., Barnes, J.C., *et al*., 2014. Induced-fit catalysis of corannulene bowl-to-bowl inversion. Nat. Chem. 6, 222–228.
93. Kroeger, A.A., Karton, A., 2021. Perylene bisimide cyclophanes as receptors for planar transition structures – catalysis of stereoinversions by shape-complementarity and noncovalent π-π interactions. Org. Chem. Front. 8, 4408–4418.
94. Kroeger, A.A., Karton, A., 2022. Perylene bisimide cyclophanes as biaryl enantiomerization catalysts – Explorations into π-π catalysis and host–guest chirality transfer. J. Org. Chem. 87, 5485–5496.
95. Wang, Y., Rickhaus, M., Blacque, O., *et al*., 2022. Cooperative weak dispersive interactions actuate catalysis in a shape-selective abiological racemase. J. Am. Chem. Soc. 144, 2679–2684.
96. Koshland, D.E., 1963. Correlation of structure an function in enzyme action. Science 142, 1533–1541.
97. Ibáñez, S., Peris, E., 2020. Dimensional matching versus induced-fit distortions: Binding affinities of planar and curved polyaromatic hydrocarbons with a tetragold metallorectangle. Angew. Chem. 59, 6860–6865.
98. Karton, A., 2016. A computational chemist's guide to accurate thermochemistry for organic molecules. WIREs Comput. Mol. Sci. 6, 292–310.
99. Bursch, M., Mewes, J.-M., Hansen, A., Grimme, S., Best-Practice, D.F.T., 2022. Protocols for basic molecular computational chemistry. Angew. Chem. 134, e202205735.
100. Karton, A., Spackman, P.R., 2021. Evaluation of density functional theory for a large and diverse set of organic and inorganic equilibrium structures. J. Comput. Chem. 42, 1590–1601.
101. Weigend, F., Ahlrichs, R., 2005. Balanced basis sets of split valence, triple zeta valence and quadruple zeta valence quality for H to Rn: Design and assessment of accuracy. Phys. Chem. Chem. Phys. 7, 3297–3305.
102. Chan, B., Collins, E., Raghavachari, K., 2021. Applications of isodesmic-type reactions for computational thermochemistry. WIREs Comput. Mol. Sci. 11, e1501.
103. Karton, A., Schreiner, P.R., Martin, J.M.L., 2016. Heats of formation of platonic hydrocarbon cages by means of high-level thermochemical procedures. J. Comput. Chem. 37, 49–58.
104. Wheeler, S.E., 2012. Homodesmotic reactions for thermochemistry. WIREs Comput. Mol. Sci. 2, 204–220.
105. Ramabhadran, R.O., Raghavachari, K., 2011. Theoretical thermochemistry for organic molecules: Development of the generalized connectivity-based hierarchy. J. Chem. Theory Comput. 7, 2094–2103.
106. Karton, A., Martin, J.M.L., 2011. Basis set convergence of explicitly correlated double-hybrid density functional theory calculations. J. Chem. Phys. 135, 144119.
107. Morgante, P., Peverati, R., 2020. The devil in the details: A tutorial review on some undervalued aspects of density functional theory calculations. Int. J. Quantum Chem. 120, e26332.
108. Goerigk, L., Mehta, N., 2019. A trip to the density functional theory zoo: Warnings and recommendations for the user. Aust. J. Chem. 72, 563–573.
109. Makkar, P., Ghosh, N.N., 2021. A review on the use of DFT for the prediction of the properties of nanomaterials. RSC Adv. 11, 27897–27924.
110. Kiely, E., Zwane, R., Fox, R., Reilly, A.M., Guerin, S., 2021. Density functional theory predictions of the mechanical properties of crystalline materials. CrystEngComm 23, 5697–5710.
111. Wu, X., Kang, F., Duan, W., Li, J., 2019. Density functional theory calculations: A powerful tool to simulate and design high-performance energy storage and conversion materials. Prog. Nat. Sci. 29, 247–255.
112. Jain, A., Shin, Y., Persson, K.A., 2016. Computational predictions of energy materials using density functional theory. Nat. Rev. Mater. 1, 15004.
113. Tang, Q., Zhou, Z., Chen, Z., 2015. Innovation and discovery of graphene-like materials via density-functional theory computations. WIREs Comput. Mol. Sci. 5, 360–379.
114. Cohen, A.J., Mori-Sánchez, P., Yang, W., 2011. Challenges for density functional theory. Chem. Rev. 112, 289–320.
115. Peverati, R., Truhlar, D.G., 2014. Quest for a universal density functional: The accuracy of density functionals across a broad spectrum of databases in chemistry and physics. Phil. Trans. R. Soc. A 372, 20120476.

116. Mardirossian, N., Head-Gordon, M., 2017. Thirty years of density functional theory in computational chemistry: An overview and extensive assessment of 200 density functionals. Mol. Phys. 115, 2315–2372.
117 Goerigk, L., Hansen, A., Bauer, C., *et al.*, 2017. A look at the density functional theory zoo with the advanced GMTKN55 database for general main group thermochemistry, kinetics and noncovalent interactions. Phys. Chem. Chem. Phys. 19, 32184–32215.
118. Karton, A., Daon, S., Martin, J.M.L., 2011. W4-11: A high-confidence dataset for computational thermochemistry derived from W4 ab initio data. Chem. Phys. Lett. 510, 165–178.
119. Perdew, J.P., Schmidt, K., 2011. In: Van Doren, V., Van Alsenoy, C., Geerlings, P. (Eds.), Functional theory Density Functional Theory and its Application to Materials, AIP Conference Proceedings vol. 577, p. 1.
120. Yu, L.-J., Sarrami, F., O'Reilly, R.J., Karton, A., 2016. Can DFT and ab initio methods describe all aspects of the potential energy surface of cycloreversion reactions? Mol. Phys. 114, 21–33.
121. Boese, A.D., Martin, J.M.L., 2004. Development of novel density functionals for thermochemical kinetics. J. Chem. Phys. 121, 3405–3416.
122. Zhao, Y., Truhlar, D.G., 2008. he M06 suite of density functionals for main group thermochemistry, thermochemical kinetics, noncovalent interactions, excited states, and transition elements: Two new functionals and systematic testing of four M06-class functionals and 12 other functionals. Theor. Chem. Acc. 120, 215–241.
123. Martin, J.M.L., Santra, G., 2020. Empirical double-hybrid density functional theory: A 'Third Way' in between WFT and DFT. Isr. J. Chem. 60, 787–804.
124. Piras, A., Ehlert, C., Gryn'ova, G., 2021. Sensing and sensitivity: Computational chemistry of graphene-based sensors. WIREs Comput. Mol. Sci. e1526.
125. Ershova, O.V., Lillestolen, T.C., Bichoutskaia, E., 2010. Study of polycyclic aromatic hydrocarbons adsorbed on graphene using density functional theory with empirical dispersion correction. Phys. Chem. Chem. Phys. 12, 6483–6491.
126. Lechner, C., Sax, A.F., 2014. Adhesive forces between aromatic molecules and graphene. J. Phys. Chem. C 118, 20970–20981.
127. Ha, M., Kim, D.Y., Li, N., *et al.*, 2017. Adsorption of carbon tetrahalides on coronene and graphene. J. Phys. Chem. C 121, 14968–14974.
128. Kroeger, A.A., Karton, A., 2022. Graphene-induced planarization of cyclooctatetraene derivatives. J. Comput. Chem. 43, 96–105.
129. Yönder, Ö., Schmitz, G., Hättig, C., *et al.*, 2020. Can small polyaromatics describe their larger counterparts for local reactions? A computational study on the H-abstraction reaction by an H-atom from polyaromatics. J. Phys. Chem. A 124, 9626–9637.
130. Zarudnev, E., Stepanian, S., Adamowicz, L., Karachevtsev, V., 2016. Noncovalent interaction of graphene with heterocyclic compounds: Benzene, imidazole, tetracene, and imidazophenazines. ChemPhysChem 17, 1204–1212.
131. Feng, C., Lin, C.S., Fan, W., Zhang, R.Q., van Hove1, M.A., 2009. Stacking of polycyclic aromatic hydrocarbons as prototype for graphene multilayers, studied using density functional theory augmented with a dispersion term. J. Chem. Phys. 131, 194702.
132. Mackie, I.D., DiLabio, G.A., 2008. Interactions in large, polyaromatic hydrocarbon dimers: Application of density functional theory with dispersion corrections. J. Phys. Chem. A 112, 10968–10976.
133. Karadakov, P.B., 2016. Do large polycyclic aromatic hydrocarbons and graphene bend? How popular theoretical methods complicate finding the answer to this question. Chem. Phys. Lett. 646, 190–196.
134. Karton, A., 2023. Planarization of negatively curved [7]circulene on a graphene monolayer. Chem. Phys. xxx, xx–xx.
135. Kim, K., Santos, E.J., Lee, T.H., Nishi, Y., Bao, Z., 2015. Epitaxially grown strained pentacene thin film on graphene membrane. Small 11, 2037–2043.
136. Xiao, K., Deng, W., Keum, J.K., *et al.*, 2013. Surface-induced orientation control of CuPc molecules for the epitaxial growth of highly ordered organic crystals on graphene. J. Am. Chem. Soc. 135, 3680–3687.
137. Ogawa, Y., Niu, T., Wong, S.L., *et al.*, 2013. Self-assembly of polar phthalocyanine molecules on graphene grown by chemical vapor deposition. J. Phys. Chem. C 117, 21849–21855.
138. Lee, W.C., Kim, K., Park, J., *et al.*, 2015. Graphene-templated directional growth of an inorganic nanowire. Nat. Nanotechnol. 10, 423–428.
139. Karton, A., Chan, B., Raghavachari, K., Radom, L., 2013. Evaluation of the heats of formation of corannulene and C_{60} by means of high-level theoretical procedures. J. Phys. Chem. A 117, 1834–1842.
140. Petrukhina, M.A., Andreini, K.W., Mack, J., Scott, L.T., 2005. X-ray quality geometries of geodesic polyarenes from theoretical calculations: What levels of theory are reliable? J. Org. Chem 70, 5713–5716.
141. Dobrowolski, M.A., Ciesielski, A., Cyranski, M.K., 2011. On the aromatic stabilization of corannulene and coronene. Phys. Chem. Chem. Phys. 13, 20557–20563.
142. Seiders, T.J., Baldridge, K.K., Elliott, E.L., Grube, G.H., Siegel, J.S., 1999. Synthesis and quantum mechanical structure of sym-pentamethylcorannulene and decamethylcorannulene. J. Am. Chem. Soc. 121, 7439–7440.
143. Seiders, T.J., Baldridge, K.K., Grube, G.H., Siegel, J.S., 2001. Structure/energy correlation of bowl depth and inversion barrier in corannulene derivatives: Combined experimental and quantum mechanical analysis. J. Am. Chem. Soc. 123, 517–525.
144. Lovas, F.J., McMahon, R.J., Grabow, J.U., *et al.*, 2005. Interstellar chemistry: A strategy for detecting polycyclic aromatic hydrocarbons in space. J. Am. Chem. Soc. 127, 4345–4349.
145. Grimme, S., Antony, J., Schwabe, T., Muck-Lichtenfeld, C., 2007. Density functional theory with dispersion corrections for supramolecular structures, aggregates, and complexes of (bio)organic molecules. Org. Biomol. Chem. 5, 741–758.
146. Martin, J.W., Slavchov, R.I., Yapp, E.K.Y., *et al.*, 2017. The polarization of polycyclic aromatic hydrocarbons curved by Pentagon Incorporation: The role of the flexoelectric dipole. J. Phys. Chem. C 121, 27154–27163.
147. Santra, G., Sylvetsky, N., Martin, J.M.L., 2019. Minimally empirical double-hybrid functionals trained against the GMTKN55 database: revDSD-PBEP86-D4, revDOD-PBE-D4, and DOD-SCAN-D4. J. Phys. Chem. A 123, 5129–5143.
148. Martin, J.M.L., Santra, G., 2019. Empirical double-hybrid density functional theory: A 'Third Way' in between WFT and DFT. Isr. J. Chem. 60, 787–804.
149. Goerigk, L., Sharma, R., 2016. The INV24 test set: How well do quantum-chemical methods describe inversion and racemization barriers? Can. J. Chem. 94, 1133–1143.
150. Cabaleiro-Lago, E.M., Fernández, B., Rodríguez-Otero, J., 2018. Dissecting the concave-convex π-π interaction in corannulene and sumanene dimers: SAPT(DFT) analysis and performance of DFT dispersion-corrected methods. J. Comput. Chem. 39, 93–104.
151. Sakurai, H., 2003. A synthesis of sumanene, a fullerene fragment. Science 301. (1878–1878).
152. Sakurai, H., Daiko, T., Sakane, H., Amaya, T., Hirao, T., 2005. Structural elucidation of sumanene and generation of its benzylic anions. J. Am. Chem. Soc. 127, 11580–11581.
153. Armaković, S., Armaković, S.J., Šetrajčić, J.P., Holodkov, V., 2014. Aromaticity, response, and nonlinear optical properties of sumanene modified with boron and nitrogen atoms. J. Mol. Model. 20, 2538.
154. Amaya, T., Sakane, H., Muneishi, T., Hirao, T., 2008. Bowl-to-bowl inversion of sumanene derivatives. Chem. Commun. 765–767.
155. Horn, P.R., Mao, Y., Head-Gordon, M., 2016. Probing non-covalent interactions with a second generation energy decomposition analysis using absolutely localized molecular orbitals. Phys. Chem. Chem. Phys. 18, 23067–23079.
156. Mao, Y., Horn, P.R., Head-Gordon, M., 2017. Energy decomposition analysis in an adiabatic picture. Phys. Chem. Chem. Phys. 19, 5944–5958.
157. Moustafa, G.A.I., Oki, Y., Akai, S., 2018. Lipase-catalyzed dynamic kinetic resolution of C1- and C2-symmetric racemic axially chiral 2,2'-dihydroxy-1,1'-biaryls. Angew. Chem. Int. Ed. 57, 10278–10282.
158. Ma, G., Deng, C., Deng, J., Sibi, M.P., 2018. Dynamic kinetic resolution of biaryl atropisomers by chiral dialkylaminopyridine catalysts. Org. Biomol. Chem. 16, 3121–3126.
159. Staniland, S., Adams, R.W., McDouall, J.J.W., *et al.*, 2016. Biocatalytic dynamic kinetic resolution for the synthesis of atropisomeric biaryl N-oxide Lewis base. Catalysts. Angew. Chem. Int. Ed. 55, 10755–10759.

160. Gustafson, J.L., Lim, D., Miller, S.J., 2010. Dynamic kinetic resolution of biaryl atropisomers via peptide-catalyzed asymmetric bromination. Science 328, 1251–1255.
161. Zhao, Y., Truhlar, D.G., 2005. Design of density functionals that are broadly accurate for thermochemistry, thermochemical kinetics, and nonbonded interactions. J. Phys. Chem. A 109, 5656–5667.
162. Colter, A.K., Clemens, L.M., 1964. Solvent effects in the racemization of 1,1'-binaphthyl. A note on the influence of internal pressure on reaction rates. J. Phys. Chem. 68, 651–654.
163. Cooke, A.S., Harris, M.M., 1967. Optical activity in the 1,1'-binaphthyl series. Energy barriers to racemisation of 8-substituted 1,1'-binaphthyls. J. Chem. Soc. C 0, 988–992.
164. Parmar, D., Sugiono, E., Raja, S., Rueping, M., 2014. Complete field guide to asymmetric BINOL-phosphate derived brønsted acid and metal catalysis: History and classification by mode of activation; Brønsted acidity, hydrogen bonding, ion pairing, and metal phosphates. Chem. Rev. 114, 9047–9153.
165. Brunel, J.M., 2007. Update 1 of: BINOL: A versatile chiral reagent. Chem. Rev. 107, PR1–PR45.
166. Chen, Y., Yekta, S., Yudin, A.K., 2003. Modified BINOL ligands in asymmetric catalysis. Chem. Rev. 103, 3155–3212.
167. Ma, G., Sibi, M.P., 2015. Catalytic kinetic resolution of biaryl compounds. Chem. Eur. J. 21, 11644–11657.
168. Jolliffe, J.D., Armstrong, R.J., Smith, M.D., 2017. Catalytic enantioselective synthesis of atropisomeric biaryls by a cation-directed O-alkylation. Nat. Chem. 9, 558–562.
169. Patel, D.C., Woods, R.M., Breitbach, Z.S., Berthod, A., Armstrong, D.W., 2017. Thermal racemization of biaryl atropisomers. Tetrahedron: Asymmetry 28, 1557–1561.
170. Kyba, E.P., Gokel, G.W., De Jong, F., *et al.*, 1977. Host-guest complexation. 7. The binaphthyl structural unit in host compounds. J. Org. Chem. 42, 4173–4184.
171. Johansson, M.P., Olsen, J., 2008. Torsional barriers and equilibrium angle of biphenyl: Reconciling theory with experiment. J. Chem. Theory Comput. 4, 1460–1471.
172. Hirano, M., Komine, N., Arata, E., *et al.*, 2019. Recent advances of achiral and chiral diene ligands in transition-metal catalyses. Tetrahedron Lett. 60, 150924.
173. Melcher, M.-C., Ivsic, T., Olagnon, C., *et al.*, 2018. Control of enantioselectivity in rhodium(I) catalysis by planar chiral dibenzo[a,e]cyclooctatetraenes. Chem. Eur. J. 24, 2344–2348.
174. Wender, P.A., Lesser, A.B., Sirois, L.E., 2012. Rhodium dinaphthocyclooctatetraene complexes: Synthesis, characterization and catalytic activity in [5 + 2] cycloadditions. Angew. Chem. Int. Ed. 51, 2736–2740.
175. Tokizaki, C., Yoshida, T., Takayanagi, T., 2016. Quantum transition state dynamics of the cyclooctatetraene unimolecular reaction on ab initio potential energy surfaces. Chem. Phys. 469, 97–104.
176. Andres, J.L., Castano, O., Morreale, A., Palmeiro, R., Gomperts, R., 1998. Potential energy surface of cyclooctatetraene. J. Chem. Phys. 108, 203–207.
177. Schild, A., Paulus, B., 2013. Multireference calculations for ring inversion and double bond shifting in cyclooctatetraene. J. Comput. Chem. 34, 1393–1397.
178. Huang, H., Stewart, T., Gutmann, M., *et al.*, 2009. To flip or not to flip? Assessing the inversion barrier of the tetraphenylene framework with enantiopure 2,15-dideuteriotetraphenylene and 2,7-dimethyltetraphenylene. J. Org. Chem. 74, 359–369.
179. Bachrach, S.M., 2009. Tetraphenylene ring flip revisited. J. Org. Chem. 74, 3609–3611.
180. Shen, Y., Chen, C.-F., 2012. Helicenes: Synthesis and applications. Chem. Rev. 112, 1463–1535.
181. Lakshman, M.K., Kole, P.L., Chaturvedi, S., *et al.*, 2000. Methyl group-induced helicity in 1,4-dimethylbenzo[c]phenanthrene and its metabolites: Synthesis, physical, and biological properties. J. Am. Chem. Soc. 122, 12629–12636.
182. Cioslowski, J., Liu, G., Martinov, M., Piskorz, P., Moncrieff, D., 1996. Energetics and site specificity of the homolytic C-H bond cleavage in benzenoid hydrocarbons: An ab initio electronic structure study. J. Am. Chem. Soc. 118, 5261–5264.